J. Appl. Cryst. (1999). **32**, 322–326

Quantitative treatment for extracting coherent elastic scattering from X-ray scattering experiments

Khalid Laaziri,[a] J. L. Robertson,[b] S. Roorda,[a]* M. Chicoine,[a] S. Kycia,[c] J. Wang[d]† and S. C. Moss[d]

[a]*Groupe de Recherche en Physique et Technologie des Couches minces, Département de Physique, Université de Montréal, CP 6128 Succursale Centre-Ville, Montréal (QC), H3C 3J7, Canada,* [b]*Solid State Division, Oak Ridge National Laboratory, PO Box 2008, Oak Ridge, TN 37831-6393, USA,* [c]*CHESS, Wilson Laboratory, Cornell University, Ithaca, NY 14853, USA, and* [d]*Department of Physics, University of Houston, Houston (TX) 77204-5506, USA. E-mail: roorda@lps.umontreal.ca*

(*Received 25 May 1998; accepted 27 October 1998*)

Abstract

A fitting procedure for separating the inelastic and elastic contributions to the total scattering in diffuse-scattering experiments at high energy using energy-dispersive X-ray techniques is presented. An asymmetric peak function is used to model the elastic peak. The inelastic scattering peak is modeled using a theoretical Compton profile, calculated using the impulse approximation (Hartree–Fock wave functions were used), convoluted with the detector resolution. This procedure, which requires only two free parameters, is shown to be extremely effective in extracting the integrated elastic intensity of coherent scattering at each wave vector, even at low scattering angles where the Compton scattering is not well resolved.

1. Introduction

The scattering by atoms of X-rays with energies less than 100 keV consists of two main processes. One is the coherent elastic or 'Thomson' scattering which occurs when the energy of the incident photon is unchanged after interacting with the atom. This scattering process is responsible for the Bragg reflections that provide information on the atomic structure of a material. The other process is incoherent inelastic or 'Compton' scattering. Here the energy of the incident photon is changed after colliding with the atom. For example, a free electron at rest will scatter a photon according to

$$\lambda - \lambda_i = 0.02426(1 - \cos 2\theta) \qquad (1)$$

where λ_i is the incident wavelength, which arises directly from energy and momentum conservation, and 2θ is the scattering angle. However, the electrons in the atoms are not at rest; therefore the Compton scattering leads to a distribution of scattered energies superposed on the elastically scattered signal. Here we include as elastic the scattering arising from the thermal motion when the energy transfer is very small (meV) compared to the incident energy (keV).

Advances in X-ray sources and instrumentation have allowed scattering measurements to be extended to much larger values of Q ($Q = 4\pi \sin\theta/\lambda$). By using 60 keV X-rays, data have been collected to Q as high as 60 Å^{-1}, which provides an extremely high real-space resolution of the local atomic structure of crystalline and amorphous materials. In fact, we have applied the procedure described in this paper to the measurement of the radial distribution function (RDF) of pure amorphous material studied at the CHESS 24-pole wiggler A2 station. As will be shown in forthcoming publications, the combination of a specially prepared sample (very high purity, 10 µm thick, homogeneous edge-supported amorphous silicon), large Q range (0.5–55 Å^{-1}) and a careful analysis, as described here, leads to an RDF of unprecedented precision and resolution.

Such high-energy X-rays scattered by thin films have the additional advantage that multiple scattering is negligible; however, the new difficulty is the large contribution from the Compton scattering to the total scattering. For amorphous materials composed of light atoms, the Compton contribution to the total scattering is often larger than the coherent contribution. In order to extract the integrated elastic scattering, it is important to separate the Compton from the elastic scattering for each value of Q. Many different approaches have been used to resolve this problem. An analyzer crystal with a narrow energy band pass can be used to remove some of the Compton scattering at larger scattering angles, but at low angles the two scattering contributions begin to overlap in energy and cannot be separated in this fashion. Another method consists of collecting the total scattering, normalizing to absolute units, and subtracting the tabulated value for the Compton contribution (*International Tables for X-ray Crystallography*, 1995). There is also the fluorescence excitation method of Warren & Mavel (1965). While in principle these

† Present address: NASA, Houston, TX, USA.

methods will yield an adequate removal of the Compton scattering, in practice great difficulty is encountered when the Compton contribution is large compared to the elastic scattering or when the scattering angle is small. More recently a very useful method has been developed by Ice & Sparks (1990), in which a curved mosaic analyzer crystal focuses the scattered X-rays onto a position-sensitive detector (PSD), thereby displaying both elastic and inelastic intensity on a multichannel analyzer. This technique has proved quite useful in the removal of Compton scattering from the diffuse scattering from amorphous materials (Cheng *et al.*, 1994) and disordered crystalline alloys (Reinhard *et al.*, 1992). Its energy resolution is excellent, but it becomes impractical at the very high X-ray energies employed in the present series of experiments.

For our purpose it has proven best to collect the energy spectrum of the total scattering using a germanium solid-state detector with a considerably lower energy resolution than that obtained for lower energy using the Ice–Sparks detector (Ice & Sparks, 1990). The scans were performed in reflection and transmission geometry with a fixed incident sample position, and fixed energies of 13, 21.74 and 43.6 keV, and by varying the scattering angle 2θ. The germanium detector was calibrated and its resolution was determined using a selection of suitable radioactive sources. The apparent loss of resolution is actually quite acceptable given the extended range of our scans which, as we shall see, permits the complete separation of the Compton and elastic components at high angles for high energy X-rays. At these energies and angles the analyzer/PSD arrangement cannot properly cover the relevant energy range. Curve fitting of the energy spectrum scattering can then be used to separate the elastic and inelastic contributions. In the following section, we present an accurate and efficient method for modeling the energy spectrum. An asymmetric peak function is used to fit the elastic contribution, and a calculated Compton profile is used to fit the inelastic contribution to the total scattering.

2. Compton scattering

The energy spectrum of the Compton scattering is calculated using the impulse approximation (Dumond, 1929; Eisenberger & Platzman, 1970). The Hamiltonian for the interaction of the radiation field with a non-relativistic electrically charged particle is given by

$$H = \frac{e}{m_0 c}\mathbf{p}.\mathbf{A} + \frac{e^2}{2m_0c^2}\mathbf{A}.\mathbf{A} \tag{2}$$

by retaining only the A^2 terms in the perturbation theory expression. Using Fermi's golden rule, the cross section for Compton scattering (Eisenberger & Platzman, 1970) is

$$\frac{\mathrm{d}^2\sigma}{\mathrm{d}\omega\mathrm{d}\Omega} = \left(\frac{e^2}{m_0c^2}\right)^2\left(\frac{1+\cos^2 2\theta}{2}\right)\left(\frac{\omega_2}{\omega_1}\right) \times \sum_2 |\langle\Psi_2|\exp(i\mathbf{kr})|\Psi_1\rangle|^2\delta(E_2 - E_1 - \omega) \tag{3}$$

where m_0 is the electron rest mass, 2θ is the scattering angle, ω_1 the incident photon energy, ω_2 the scattered photon energy, and Ψ_1 and Ψ_2 are respectively the wave functions for the electron in its initial bound state and its final continuum state.

The impulse approximation assumes that the electrons responsible for scattering the photons may be treated as free rather than bound. However, orbital effects are included in so far as they produce a spread in the initial free electron momenta. The cross section for Compton scattering in this approximation is

$$\frac{\mathrm{d}^2\sigma}{\mathrm{d}\omega\mathrm{d}\Omega} = \left(\frac{e^2}{m_0c^2}\right)^2\left(\frac{1+\cos^2 2\theta}{2}\right)\left(\frac{\omega_2}{\omega_1}\right)\left(\frac{m_0}{|k|}\right)J(q) \tag{4}$$

where k is the momentum transfer, $J(q)$ is the Compton profile (Biggs *et al.*, 1975), and q is the projection of p_1 (the individual electron momentum before collision upon a unit vector in the direction of the momentum transfer $\mathbf{k} = \mathbf{k}_1 - \mathbf{k}_2$, where $\mathbf{k}_1$ is the incident wave vector and $\mathbf{k}_2$ the outgoing wave vector) and is proportional to the separation from the center of the Compton line for scattering from a free electron at rest. q is expressed in atomic units of $me2/\hbar$, which is the average electron momentum in the ground state of hydrogen,

$$q = -\frac{\mathbf{k}.\mathbf{p}_1}{|k|} = -137\frac{\omega_1 - \omega_2 - \omega_1\omega_2[(1-\cos 2\theta)/m_0c^2]}{(\omega_1^2 + \omega_2^2 - 2\omega_1\omega_2\cos 2\theta)^{1/2}}. \tag{5}$$

$$J(q) = \tfrac{1}{2}\int_q^\infty \frac{I(p)}{p}\mathrm{d}p \tag{6}$$

$I(p)$ is the electron momentum density for electrons of momentum p.

The impulse-approximation Compton profiles (IACPs) calculated numerically in this paper are based on the work of Biggs *et al.* (1975) using the non-relativistic and relativistic Hartree–Fock wavefunctions of Mann (Mann & Waber, 1973; Mann, 1973). The routine for generating IACPs may be obtained on request from the authors (K. Laaziri, S. Roorda). Fig. 1 shows an example of the IACP for $2\theta = 65^\circ$ and an incident energy of 43.6 keV.

3. Thomson scattering

An analytical asymmetric peak function (available in most curve-fitting software) was used to describe the elastic scattering. Due to the asymmetry of the coherent scattering, probably arising from the focusing and monochromating system, common peak-fit functions cannot adequately reproduce the tails of the elastic peak. The following analytical asymmetric peak function gave satisfactory results:

$$a_0 \exp[(a_1 - a_2 \ln a_3 - x)/a_2]\{1 + \exp[(a_1 - a_2 \ln a_3 - x)/a_2]\}^{-a_3-1} a_3^{-a_3} (a_3 + 1)^{a_3+1} \quad (7)$$

where a_0, a_1, a_2 and a_3 are, respectively, the height, center, width, and shape of the peak. Fig. 2 shows an example of this analytical peak function.

4. Fitting procedure

The curve fitting procedure consists of five steps. (i) Select an energy spectrum collected at large scattering angle in which the elastic and the Compton contributions are well separated (see Fig. 3). (ii) Calculate the corresponding IACP. (iii) Fit the spectrum to determine the Compton amplitude, the elastic peak amplitude (a_0), center (a_1), width (a_2) and shape (a_3). (iv) For all other values of Q, calculate the corresponding IACP, and fit to determine the amplitude of the Compton and the elastic contribution, while keeping a_1, a_2 and a_3 fixed. (v) For each spectrum, subtract the Compton contribution and integrate to obtain the elastic scattering.

Of course, the first step can be carried out for several spectra collected at large scattering angles in order better to determine the parameters a_1, a_2 and a_3.

Figs. 4 and 5 show some typical fits to energy spectra collected at different scattering angles. We note that with this curve fitting procedure, even when the inelastic and elastic peaks are not well resolved, smooth fits can still be obtained, as can be seen from Fig. 6.

The fitting function used was

$$F(x) = E(x) + C_0(x) \quad (8)$$

where $E(x)$ is the elastic fitting function (7) with a_0 as the only free parameter, and $C_0(x)$ is the Compton fitting function, expressed as

$$C_0(x) = N \times \text{spline}(x) \quad (9)$$

where spline(x) is a spline fit of the calculated IACP and N is a fitting parameter for the Compton amplitude. The theoretical IACP, convoluted with the detector resolution, gives the correct shape of the Compton scattering

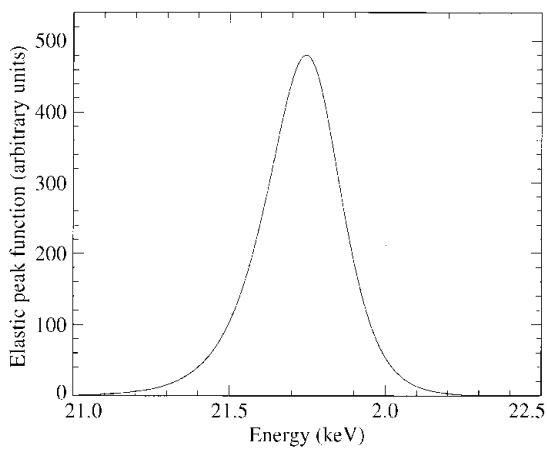

Fig. 2. Asymmetric elastic peak function for an energy of 21.75 keV.

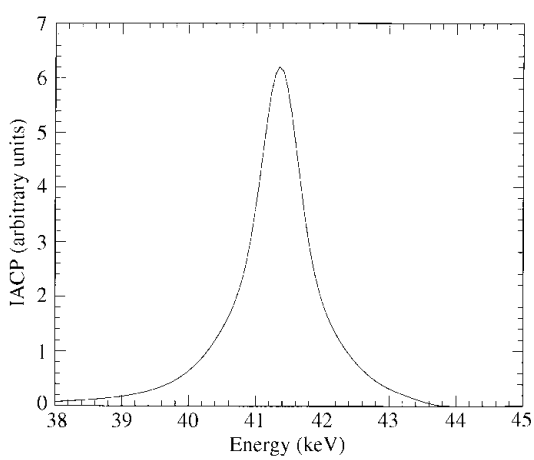

Fig. 1. Impulse-approximation Compton profile calculated for 43.6 keV incident X-rays scattered through 90° by amorphous silicon.

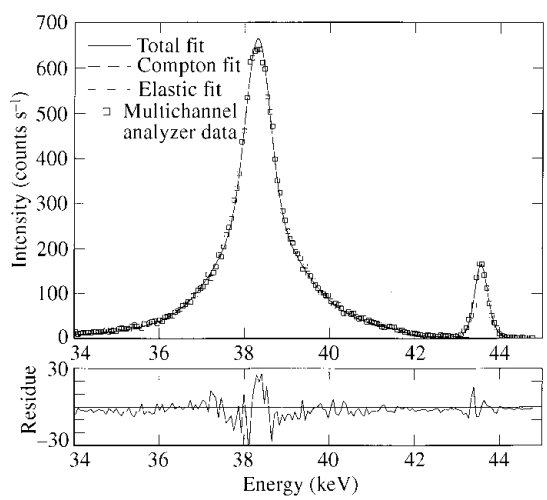

Fig. 3. Fit of the total X-ray scattering energy spectra at Q = 40 Å^{-1} (E = 43.6 keV).

peak; therefore the only other free parameter (besides a_0) is the Compton scattering amplitude N.

The importance of this procedure is that no systematic errors are introduced during the evaluation of the integrated intensity of the elastic peak. This is not the case for the single-channel analyzer (SCA) technique, in which discriminator windows are set on the elastic scattering peak so as to exclude incoherent Compton scattering. One can easily show that this method introduces a systematic error varying with 2θ, compared to the method presented here, due to an indeterminent amount of the incoherent scattering entering the detector. Table 1 shows the integrated intensity of the elastic scattering peak for different scattering angles, observed during our X-ray diffraction experiment on pure amorphous silicon. Data collected with the solid-state detector were output simultaneously to the multichannel analyzer and an SCA with the discriminator window centered on the elastic energy. In the second column of Table 1, we present the intensity (integrated over the energy window) from the SCA, and in the third column the integrated intensity is deduced from our curve-fitting procedure. At low scattering angle, when the peak separation between the elastic and Compton scattering becomes very small, the Compton scattering contributes a substantial amount to the counts within the SCA discriminator window. The error in evaluating

Table 1. *Elastic intensity from an SCA discriminator compared with that from the curve-fitting procedure*

The table presents the systematic error introduced into the coherent elastic intensity by using an SCA discriminator with the energy window centered on the elastic energy as compared with fitting the energy spectrum, for an incident energy of 21.74 keV.

2θ (°)	Elastic intensity from discriminator window (counts)	Elastic intensity from curve fitting (counts)	Error (%) in elastic intensity from discriminator
129	1090	1075	1.4
116	1320	1300	1.5
104	1313	1292	1.6
94	1632	1601	1.9
85	2210	2120	4.2
77	2729	2569	6.2
68	2900	2637	9.9
61	3869	3352	15
53	5185	4182	24
46	7158	5189	38

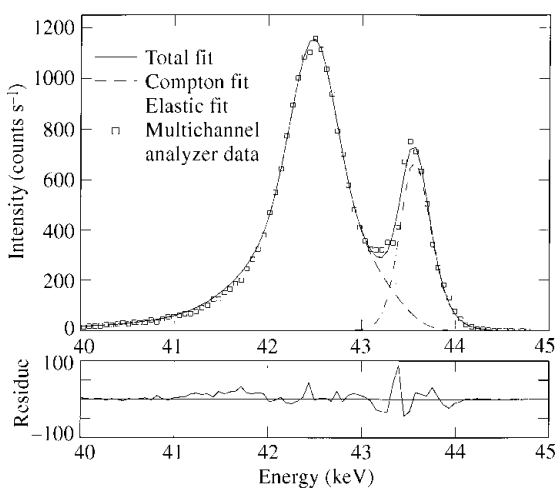

Fig. 4. Fit of the total X-ray scattering energy spectra at Q = 20 Å^{-1} (E = 43.6 keV).

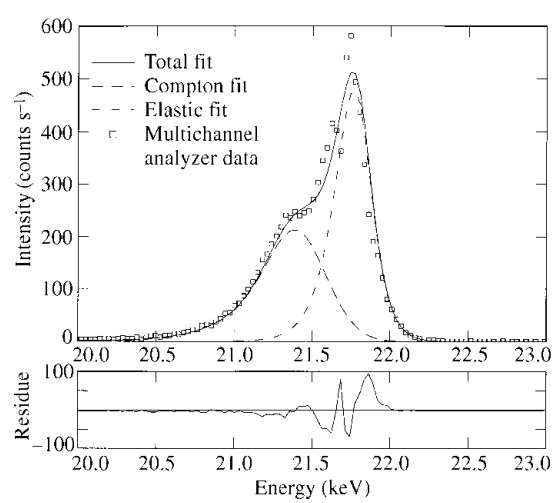

Fig. 5. Fit of the total X-ray scattering energy spectra at Q = 10 Å^{-1} (E = 21.74 keV).

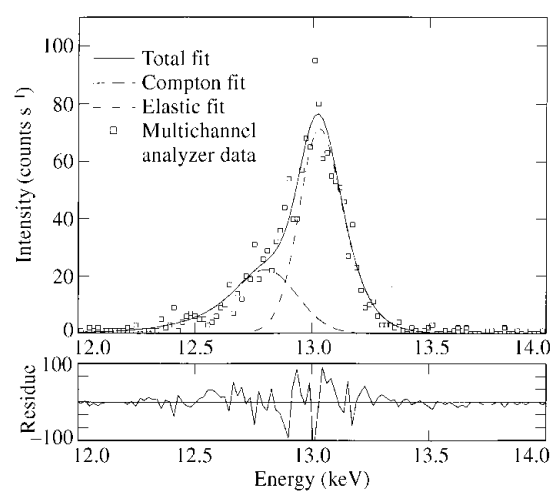

Fig. 6. Fit of the total X-ray scattering energy spectra at Q = 7 Å^{-1} (E = 13 keV).

the true elastic scattering count is plotted in Fig. 7. The systematic error introduced by not discriminating against the Compton contribution increases rapidly towards low scattering angles. This is of great concern because the RDF, especially the RDF at short range, is very sensitive to systematic errors in the diffracted intensity which vary slowly with Q. Therefore, errors such as those shown in Fig. 7 may be expected to compromise seriously those RDFs that are determined using only an SCA to suppress the Compton contributions to the total signal. By using the method described in this paper, *i.e.* measuring and fitting the energy spectrum at each value of Q, such errors can be avoided and a clean and unambiguous elastic scattering profile can be attained.

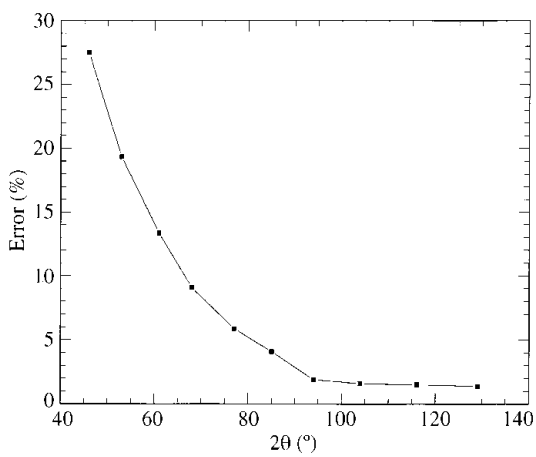

Fig. 7. Systematic error in the integrated elastic scattering intensity introduced by using a fixed discriminator energy window.

5. Conclusions

An efficient curve-fitting procedure for energy spectra in X-ray scattering has been presented in this paper. This curve-fitting method allows the separation of the elastic and inelastic (Compton) scattering intensities, even at very low scattering angles where these signals are not fully resolved experimentally.

This work is supported by the Natural Science and Engineering Research Council of Canada (NSERC) and the Fonds pour la formation de Chercheurs et l'Aide à la Recherche (FCAR). This work is based upon research conducted at the Cornell High Energy Synchrotron Source (CHESS), which is supported by the National Science Foundation, under Award No. DMR-9311772. At the University of Houston, this work was supported by the US DOE/BES under contract DE-FG05_87ER 45325 and at Oak Ridge National Laboratory under contract DE-AC05_96OR 22464.

References

Biggs, F., Mendehlson, L. B. & Mann, J. B. (1975). *At. Data Nucl. Data Tab*. **16**, 201–309.
Cheng, J., Moss, S. C., Eisner, M. & Zschack, P. (1994). *Pigment Cell Res*. **7**, 255–262.
Dumond, J.W. M. (1929). *Phys. Rev.* **33**, 643–658.
Eisenberger, P. & Platzman, P. M. (1970). *Phys. Rev. A*, **2**, 415–423.
Ice, G. E. & Sparks, C. J. (1990). *Nucl. Instrum. Methods A*, **291**, 110–116.
International Tables for X-ray Crystallography (1995). Vol. C. Birmingham: Kynoch Press.
Mann, J. B. (1973). *At. Data Nucl. Data Tab*. **12**, 1–86.
Mann, J. B. & Waber, J. T. (1973). *At. Data*, **5**, 201–276
Reinhard, L., Robertson, J. L., Moss, S. C., Ice, G. E., Zschack, P. & Sparks, C. J. (1992). *Phys. Rev. B*, **45**, 2662–2670.
Warren, B. E. & Mavel, G. (1965). *Rev. Sci. Instrum.* **36**, 196–202.